We are IntechOpen, the world's leading publisher of Open Access books Built by scientists, for scientists

4,800
Open access books available

122,000
International authors and editors

135M
Downloads

Our authors are among the

154
Countries delivered to

TOP 1%
most cited scientists

12.2%
Contributors from top 500 universities

CLARIVATE ANALYTICS BOOK CITATION INDEX INDEXED

WEB OF SCIENCE™

Selection of our books indexed in the Book Citation Index in Web of Science™ Core Collection (BKCI)

Interested in publishing with us?
Contact book.department@intechopen.com

Numbers displayed above are based on latest data collected.
For more information visit www.intechopen.com

9

Many-particle Monte Carlo Approach to Electron Transport

G. Albareda, F. L. Traversa, A. Benali and X. Oriols
Departament d'enginyeria Electrònica, Universitat Autònoma de Barcelona
Spain

1. Introduction

Recent technological advances have made possible to fabricate structures at the nanoscale. Such structures have already a large range of applications in very disparate fields of science and technology, and day by day new proposals are being suggested. A particular example of is nanoelectronics, where nanostructures constitute the platforms where smaller and smaller electron devices are being designed with the aim of letting the semiconductor industry to go forward in manufacturing faster and less consuming devices.

Today, due to the increase of the complexity and cost of the technological processes necessary to fabricate electron device prototypes, precise predictions on their functionality allowing to rule out specific designs are strictly necessary. In this regard, the success of nanoelectronics partially relies on physical theories on electron transport usually implemented on computer design tools that constitute at this moment a research and development cost reduction amount of the 35%, and is expected to increase up to 40% in the next future (Sverdlov et al., 2008). But more importantly, beyond the supporting role in the progress of electronics, theoretical approaches to electron transport constitute a necessary tool to guide the continuous breakthroughs of the electronics industry.

Analytical approaches to model electron transport have been developed since the invention of the first vacuum valve (Conwell, 1967), however, it has been the improvement of electronics itself which has make it possible to intensify the research on the simulation of electron transport by means of computer-aided tools. With the aid of faster computers, it became possible to obtain exact numerical solutions of complex microscopic physical models. The first fully numerical description of electron transport was already suggested in 1964 by Gummel (Gummel, 1964) for the one-dimensional bipolar transistor. The approach was further developed and applied to *pn*-junctions (De Mari, 1968) and to avalanche transit-time diodes by Scharfetter and Gummel (Scharfetter & Gummel, 1969). It was in 1966 that the first application of the Monte Carlo (MC) method was proposed by T. Kurosawa to solve the semi-classical Boltzmann Transport Equation (BTE) (Kurosawa, 1966). Since this pioneering work, the MC technique applied to device simulation has suffered a great evolution, and over more than 30 years it has been applied to understand several physical processes related with transport phenomena in many scenarios of interest (an extend review can be found in Refs. Jacoboni & Lugli, 1989; Jacoboni & Reggiani, 1983).

The use of the MC technique in the field of nanoelectronics is justified by the enormous complexity associated to the microscopical description of electron transport in solid-state structures. Current computational limitations forces any electron transport model to restrict the entire simulated degrees of freedom to a very few number. Such a simplification of the real scenario implies the use of probabilistic distributions that provide statistical information on those parts of the system that have been neglected/approximated[1]. Here is precisely where the MC technique comes into play by providing a sequence of random numbers with such particular distribution probabilities.

The study of electron transport through the BTE constitutes, however, just a single-particle approach to the electron transport problem (Albareda, Suñé & Oriols, 2009; Di Ventra, 2008), only accurate enough to describe electron dynamics in large structures containing a large number of carriers. As electron device sizes shrink into the nanometer scale, device structures are characterized by simultaneously holding a small number of electrons in a few nanometers. In this regime, carriers experience very little or no scattering at all (ballistic limit). The Coulomb interaction among carriers becomes then particularly important because the motion of one electron strongly depends on the motion of all the others and viceversa, i.e. their dynamics get strongly correlated. Hence, a many-particle formulation of electron transport becomes mandatory.

The main thrust of this chapter is to present a generalization of the standard MC solution of the BTE by introducing a rigorous many-particle description of electron dynamics and its classical correlations.

Overview on the treatment of Coulomb correlations:

In the last decade, several works have remarked the necessity of paying maximum attention not only to electron-electron (e-e) but also to electron-impurity (e-i) Coulomb interactions when developing new approaches to electron transport (Barraud et al., 2002; Gross et al., 1999; 2000b; Wordelman & Ravaioli, 2000). In the MC solution of the BTE, historically the e-i (and also a part of the e-e) interactions have been introduced perturbatively as "instantaneous" and "local" transitions of electrons between different regions of the k-space. Such approach is clearly inappropriate at deep nanoscale because it assumes homogenous distributions of charges, so that the effects of "scattering" of electrons become position independent. The expressions for the e-e and e-i scattering rates in k-space are, in addition, based on a two-body model which accounts for many-particle contributions only through the screening function of simplified effective potentials, and which does not take into account the electrostatic effects of the gate, drain and source terminals on the potential distribution.

The standard solution to avoid such important limitations of the MC without significantly increasing the computational cost of the simulations, consists on defining an ad-hoc spatial division of the e-e and e-i interactions. For sufficiently large structures (several tens of nanometers), two distinguishable behaviors of the electrostatic potential can be identified depending on the proximity to the charges. On one hand, in a position very near ($\sim$ few nanometers) to the carriers and ions, the shape of the scalar potential behaves just like $1/r$. On the other hand, far enough from them ($\sim$ tens of nanometers), the shape of the scalar

[1] An example of these distributions is the *Fermi Dirac distribution*, which describes the way (i.e. position, time and momentum) electrons enter the active region once the simulation of the battery, leads and contacts has been avoided. Another example are, for instance, the *scattering rates* describing the interaction between electrons and the atoms conforming the underlying crystallographic mesh within the effective mass approximation.

potential depends on the particular spatial charge distribution. In this regard, a common strategy consists on introducing a long-range part of the Coulomb interaction numerically through the solution of the mesh-dependent mean-field Poisson equation, and a short-range part analytically (the so-called Monte Carlo/Molecular dynamics approach, MCMD, (Gross et al., 1999; Wordelman & Ravaioli, 2000)), or perturbativelly (Barraud et al., 2002). The MCMD approach, however, shows some inconvenients. The first reported limitation was the so-called "double counting" of the electrostatic force in the short-range interaction term (Gross et al., 1999; 2000a). Since the e-e and e-i interactions are already included, in a smoothed way, in the self-consistent solution of the Poisson equation, the addition of a separate analytical force (the Molecular dynamics term) leads to the overestimation of both the e-e and the e-i interactions (Gross et al., 1999). Such a problem can be avoided by properly identifying the spatial region where short-range Coulomb interactions have to be included. In particular, the Molecular dynamics routine uses a "corrected" short-range Coulomb interaction that excludes the long-range contribution from the Poisson equation (Gross et al., 1999; 2000a;b). The problem comes then from the analytical nature of the short-range corrections, which can lead to unphysically large forces that cause artificial heating and cooling (for acceptors and donors respectively) of the carriers (Gross et al., 2000b; Ramey & Ferry, 2003). Again, this problem can be amended by introducing modifications of the analytical expressions of the Coulomb interaction in the short-range region (Alexander et al., 2005; 2008) or by implementing density gradient (quantum) corrections that accounts for the formation of bound states in the donor induced wells (Asenov et al., 2009; Vasileska & Ahmed, 2005).

Unfortunately, even all the above improvements of the MC solution of the BTE can fail when device dimensions are aggressively reduced to a very few nanometers either in lateral or longitudinal directions. Then, separations between long- (screened) and short- (unscreened) range contributions of the Coulomb interaction become quite misleading, and moreover, under such particular conditions, an important intrinsic limitation of the MC solution of the BTE come to light: it constitutes a single-particle description of electron transport, i.e. it describes the time-evolution of the electron distribution function (i.e. the Boltzmann distribution) in a single-electron phase-space (Albareda, López, Cartoixà, Suñé & Oriols, 2010; Albareda, Saura, Oriols & Suñé, 2010; Albareda, Suñé & Oriols, 2009; Boltzmann, 1872).

Moreover, in addition to the above problems, due to the computational burden associated to the microscopic description of electron transport, the simulation of the Coulomb correlations between the electrons in the leads and those in the active region of an electron device is not always possible and the use of small simulation boxes is a mandatory requirement in modern nanoscale simulators (see Fig. 1). However, in order to correctly model the DC and/or AC conductance of nanoscale systems, one has to assure the accomplishment of "overall charge neutrality" and "current conservation" (Blanter & Büttiker, 2000; Landauer, 1992). The implementation of such requirements into nanoscale electron simulators demands some kind of reasonable description of the Coulomb interaction among the electrons inside and outside the simulation boxes. The boundary conditions on the borders of simulation boxes in electron transport approaches constitute also a complicate and active field of research. In fact, educated guesses for the boundary conditions are present in the literature when describing nanoscale electron devices with simulation boxes large enough to include the leads. However, such boundary conditions are not applicable for small simulation boxes that exclude the leads. Elaborated semi-classical electron transport simulators solving the time-dependent BTE within the MC technique commonly fix the potential at the borders of the simulation box equal to the external bias (i.e. Dirichlet boundary conditions) and assume ad-hoc modifications of

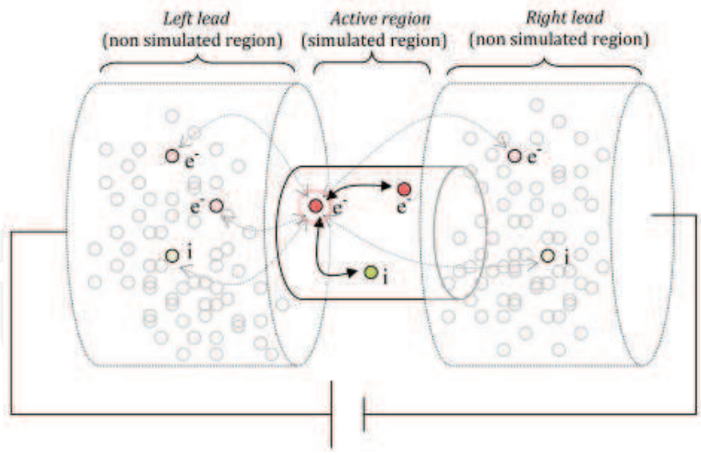

Fig. 1. Schematic representation of the Coulomb correlations among electrons in the leads and those in the active region of an electron device. e^- and i represent the conduction electrons and the ionized atoms respectively.

the injection rate to achieve "local" charge neutrality (Bulashenko et al., 1998; Fischetti & Laux, 2001; Gomila et al., 2002; Gonzalez et al., 1997; Gonzalez & Pardo, 1993; 1996; Jacoboni & Lugli, 1989; Reklaitis & Reggiani, 1999; Wordelman & Ravaioli, 2000). Some works do also include analytically the series resistances of a large reservoir which can be considered an improvement over the previous boundary conditions (Babiker et al., 1996). Other MC simulators do also consider Neumann boundary conditions (i.e. a fixed zero electric-field) (Riddet et al., 2008). The latter conditions fix also the scalar potential (up to an arbitrary constant) so that the injected charge can also be indirectly determined when a known electrochemical potential is assumed. Although all these boundary conditions are successful for large simulation boxes, they are quite inaccurate for small simulation boxes that exclude the leads (Riddet et al., 2008). In principle, there are no much computational difficulties in applying a semi-classical MC technique in large simulation boxes when dealing with mean-field approaches. However, the possibility of using smaller boxes will be very welcomed for some intensive time-consuming simulations beyond the mean-field approximation (also for statistical ensemble simulations, see Ref. Reid et al., 2009, or to compute current or voltage fluctuations that need very large simulation times to obtain reasonable estimators, see Refs. Albareda, Jiménez & Oriols, 2009; Gonzalez et al., 1997; Gonzalez & Pardo, 1993; Reklaitis & Reggiani, 1999; Wordelman & Ravaioli, 2000, etc.).

In this chapter, we are interested in revisiting the MC computation of an ensemble of Coulomb interacting particles in an open system (an electron device) without any of the approximations mentioned in the previous paragraphs. With this goal, in section 2 , we will develop an exact many-particle Hamiltonian for Coulomb interacting electrons in open systems in terms of the solutions of multiple Poisson equations (Albareda, Suñé & Oriols, 2009). To our knowledge, the type of development of the many-particle Hamiltonian proposed here has not been previously considered in the literature because, up to now, it was impossible to handle the computational burden associated with a direct solution of a many-particle Hamiltonian. Furthermore, in section 3 , we will present an original (time-dependent) boundary condition algorithm for open systems capable of accurately capturing Coulomb correlations among the electrons inside and outside the simulation box (Albareda, López, Cartoixà, Suñé & Oriols,

2010). Such boundary conditions constitute a notable improvement of standard boundary conditions used in MC approaches and, requiring a minimum computational effort, they can be implemented into time-dependent simulators with large or small simulation boxes, and for DC, AC conditions and even for the study of current (or voltage) fluctuations. Section 4 , will be devoted to present a semi-classical solution of the time-dependent many-particle Hamiltonian provided with the previous boundary conditions. This solution constitutes a generalization of the semi-classical single-particle Boltzmann distribution to many-particle systems (Albareda, López, Cartoixà, Suñé & Oriols, 2010; Albareda, Suñé & Oriols, 2009). In section 5, our many-particle MC will be used to evaluate the importance of accounting for strongly-correlate phenomena when predicting discrete doping induced effects in the channel of a quantum wire double-gate field-effect transistor (Albareda, Saura, Oriols & Suñé, 2010).

2. A Many-particle Approach to Semi-Classical Electron Transport

Although interacting many-electron systems are well assessed through the exact expression of the system's Hamiltonian, its exact solution is a very hard problem when the number of interacting electrons increase farther than a few tens. Therefore, the main difficulty that one encounters when describing electron transport at the nanoscale arises from the necessity of making reasonable approximations to an essentially untractable problem, i.e. the many-body description of electron transport.

Consider, for instance, the Hamiltonian describing a whole closed circuit, i.e. including the battery, the contacts, the leads, the active region and all the constituting elements therein (see Fig. 1). If we assume that it contains M_T electrons and $W - M_T$ atomic cores, the Hamiltonian of the system can be written as

$$\begin{aligned} H_{circuit}\left(\vec{r}_1,...,\vec{r}_G,\vec{p}_1,...,\vec{p}_G\right) = & \sum_{k=1}^{M_T}\left\{K\left(\vec{p}_k\right)+\frac{1}{2}\sum_{\substack{j=1\\ j\neq k}}^{M_T} eV_0(\vec{r}_k,\vec{r}_j)\right\} \\ & + \sum_{k=M_T+1}^{W}\left\{K\left(\vec{p}_k\right)+\frac{1}{2}\sum_{\substack{j=M_T+1\\ j\neq k}}^{W} eZ_kZ_jV_0(\vec{r}_k,\vec{r}_j)\right\} \\ & - \sum_{k=1}^{M_T}\sum_{j=M_T+1}^{W} eZ_jV_0(\vec{r}_k,\vec{r}_j), \end{aligned} \tag{1}$$

where $K\left(\vec{p}_k\right)$ is the kinetic energy of the $k-th$ particle with a momentum $\vec{p}_k$, e is the electron charge, $\vec{r}_k$ is the vector position of the k-th particle, and Z_k is the atomic number of the k-th atom. The term $V_0(\vec{r}_k,\vec{r}_j) = e/\left(4\,\pi\,\varepsilon_0\left|\vec{r}_k-\vec{r}_j\right|\right)$ is the Coulomb potential (with ε_0 the vacuum permittivity)[2].

[2] Along the whole chapter we will assume that all involved electrons are traveling at velocities much lower than light's, c (nonrelativistic approximation). Moreover, we will consider that we can neglect the electron spin-orbit coupling and that a quasi-static electromagnetic regime can be assumed. Such an assumption, however, does not means that we are considering spinless electrons. Indeed, when computing some relevant magnitudes we will account for the electron spin just by an additional factor 2. (see Ref. Albareda, López, Cartoixà, Suñé & Oriols, 2010)

2.1 The many-electron open system Hamiltonian

Notice that the solution of the Hamiltonian (1) constitute an insurmountable challenge. The reason, however, does not only reside on the huge number of variables conforming the system ($W \to \infty$), but mainly on their correlation, which does not allow to separate the dynamics of electrons. The interaction terms in (1) are the responsible of coupling each particle dynamics to the rest of particle dynamics in the system, and hence the responsible of making their solution so difficult. A common strategy to simplify the solution of equation (1) consists on reducing the involved degrees of freedom. Instead of trying to describe a whole *closed* circuit, *all* approaches to electron transport reduce the number of variables to be explicitly described by *opening* the system. As a first approach, we delimit the particles dynamics to be explicitly described to those that are free to carry electrical current.

Internally opening the system: In order to reduce the degrees of freedom in (1), we first remove their explicit dependence on the valence and core electrons by modifying the vacuum permittivity ($\varepsilon_0 \to \varepsilon = \varepsilon_r \cdot \varepsilon_0$, where ε_r is the relative permittivity) and accounting for an average induced polarization between the bounded electrons and the nuclei (Reitz et al., 1992)). We also assume the adiabatic approximation (Datta, 1995; 2005; Lundstrom & Guo, 2006) (also called Born-Oppenheimer approximation) under which conducting electrons move in a quasi-static atomic potential defined by the fixed positions of the atoms. The original Hamiltonian (1), has been then reduced to the Hamiltonian of the carriers alone:

$$H_{carriers}\left(\vec{r}_1,...,\vec{r}_M,\vec{p}_1,...,\vec{p}_M\right) = \sum_{i=1}^{M}\left\{K\left(\vec{p}_i\right)+\frac{1}{2}\sum_{\substack{j=1\\ j\neq i}}^{M} eV(\vec{r}_i,\vec{r}_j)-\sum_{j=M_T+1}^{W} eZ_jV(\vec{r}_i,\vec{R}_j)\right\} \quad (2)$$

where M is now the total number of unbounded electrons, and R_j are now the fixed positions of the atoms. The Coulomb potential,

$$V(\vec{r}_i,\vec{r}_j)=\frac{e}{4\,\pi\,\varepsilon\,\left|\vec{r}_i-\vec{r}_j\right|} \quad (3)$$

has been properly redefined according to the effective value of the dielectric permittivity. From now on, the dynamics of the nucleus and the bounded electrons are not anymore explicitly accounted for. Therefore, we do not deal with the circuit Hamiltonian, $H_{circuit}$, but with that of the M unbounded electrons (i.e. carriers), $H_{carriers}$. Although the spatial region described by $H_{carriers}$ is the same as the one described by $H_{circuit}$, we have substantially reduced its complexity by disregarding many *internal* degrees of freedom. Hence the title "internally opening the system".

We are however still dealing with a computationally insolvable problem. In order to continue reducing the degrees of freedom, an important decision to be made is that of the energy band model that will be used. Assuming the electron-atom interaction potential to be an average over a unit cell of the atomic lattice of the semiconductor, carrier kinetics can be treated almost in the same way as for free carriers, but with a modified mass called the effective mass. Such a model is thus often called the effective mass model. We define then H_0 as that part of the whole Hamiltonian containing the kinetic terms and the interaction among electrons and

atoms. We can rewrite (2) as

$$\hat{H}_{carriers} = \hat{H}_0 + \frac{1}{2}\sum_{i=1}^{M}\sum_{\substack{j=1\\ j\neq i}}^{M} eV\left(\vec{r}_i,\vec{r}_j\right), \tag{4}$$

where

$$\hat{H}_0 = \sum_{i=1}^{M} H_{0i} = \sum_{i=1}^{M}\left\{K\left(\vec{p}_i\right) - \sum_{j=M_T+1}^{G} eZ_j V\left(\vec{r}_i,\vec{R}_j\right)\right\}. \tag{5}$$

H_0 is separable and we can find monoelectronic eigenstates for every one of the M Hamiltonians H_{0i}. Moreover, if we assume an ideal periodic atomic structure, the Bloch states are solutions of these monoelectronic Hamiltonians. Considering that only one single-band is attainable by the carriers, it can be shown that the Hamiltonian (2) can be reduced to that of a many-particle envelope function (Albareda, 2010)

$$\hat{H}_{env} = \sum_{j=1}^{M}\left[K\left(\vec{p}_k\right) + \frac{1}{2}\sum_{i=1}^{M} eV\left(\vec{r}_i,\vec{r}_j\right)\right], \tag{6}$$

where $K(\vec{p}_k)$ is redefined as

$$K\left(\vec{p}_k\right) = -\frac{\hbar^2}{2}\left(\frac{\partial^2}{m_x^*\partial x_j^2} + \frac{\partial^2}{m_y^*\partial y_j^2} + \frac{\partial^2}{m_z^*\partial z_j^2}\right), \tag{7}$$

and m_x, m_y and m_z are the trace terms of the diagonalized effective mass tensor (Albareda, 2010).

The Hamiltonian in (6) is still computationally unaffordable because it involves a huge number of degrees of freedom (those of the battery, contacts, leads, etc...). In this regard, we must carry out a step forward in simplifying the described electronic system. In what follows, we spatially delimit the system to be described, i.e. we externally open the electronic system.

Externally opening the system: We divide the previous ensemble of M particles into a sub-ensemble of $N(t)$ particles whose positions are inside the volume Ω and a second sub-ensemble, $\{N(t)+1,...,M\}$ which are outside (see figure 2). We assume that the number of particles inside, $N(t)$, is a time-dependent function that provides an explicit time-dependence to the many-particle (open-system) Hamiltonian. As drawn in figure 2, we define a parallelepiped where the six rectangular surfaces $S = \left\{S^1, S^2, ..., S^6\right\}$ are the boundaries of Ω. We use $\vec{r}^{\,l}$ as the "boundary" vector representing an arbitrary position on the surfaces S^l. Now, the number of carriers in the system $N(t)$ will vary with time, i.e.

$$\hat{H}_{env}^{open}(\vec{r}_1,..,\vec{r}_M,\vec{p}_1,..,\vec{p}_{N(t)},t) = \sum_{k}^{N(t)}\left\{K\left(\vec{p}_k\right) + \frac{1}{2}\sum_{\substack{k=1\\ k\neq j}}^{N(t)} eV(\vec{r}_k,\vec{r}_j) + \sum_{j=N(t)+1}^{M} eV(\vec{r}_k,\vec{r}_j)\right\} \tag{8}$$

As we will be discussed below, the third term in (8) can be included in the Hamiltonian of the open system through the boundary conditions of the Poisson equation. The roughness of the approximation bringing together the effects of all the external particles over the $N(t)$ carriers

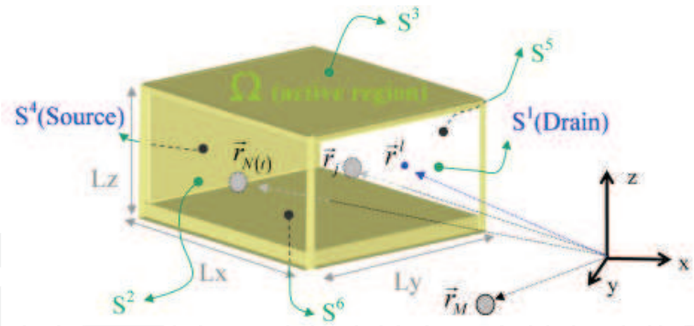

Fig. 2. Schematic representation of the open volume $\Omega = Lx \cdot Ly \cdot Lz$ and its limiting surface $S = \{S^1, S^2, ..., S^6\}$. There are $N(t)$ particles inside and $M - N(t)$ outside this volume. The vector $\vec{r}^{\,l}$ points to an arbitrary position at the boundary surface S^l. We consider S^4 and S^1 as "opened" surfaces because there is a flux of particles through them. The rest of the surfaces are "closed" borders.

will depend on our ability of formulating the boundary conditions at the borders of the active region of the electron device (see Section 3 for an extent discussion on this point). Since we will only work with the many-particle open system Hamiltonian (8), in order to simplify the notation let us simply refer to it as $\hat{H}$.

In the previous paragraphs, the assumption of a series of approximations have make it possible to go from the complex circuit Hamiltonian described in equation (1), to the much more simple one describing the "interesting" region of the circuit (8). However, although we have discussed the many-particle Hamiltonian in terms of the Coulomb force, this approach is inconvenient to deal with solid-state scenarios with a spatial-dependent permittivity (Javid & Brown, 1963). For this reason, in what follows we rewrite the many-particle Hamiltonian (8) in terms of the more generic Poisson equation, which can be applied to systems with a spatial-dependent permittivity (by simply substituting $\varepsilon \rightarrow \varepsilon(\vec{r})$). We start by rewriting the previous many-particle open system Hamiltonian (8) as:

$$H(\vec{r}_1,..,\vec{r}_M,\vec{p}_1,..,\vec{p}_{N(t)},t) = \sum_{k=1}^{N(t)} \left\{ K(\vec{p}_k) + \sum_{\substack{j=1 \\ j\neq k}}^{N(t)} e \cdot V(\vec{r}_k,\vec{r}_j) + \sum_{j=N(t)+1}^{M} e \cdot V(\vec{r}_k,\vec{r}_j) - \frac{1}{2} \sum_{\substack{j=1 \\ j\neq k}}^{N(t)} e \cdot V(\vec{r}_k,\vec{r}_j) \right\}. \quad (9)$$

Each term $V(\vec{r}_k,\vec{r}_j)$ that appears in (9) can be explicitly obtained from a Poisson (or Laplace) equation inside the volume Ω. Using the superposition property of the Poisson equation, we can rewrite (9) as:

$$H(\vec{r}_1,..,\vec{r}_{N(t)},\vec{p}_1,..,\vec{p}_{N(t)},t) = \sum_{k=1}^{N(t)} \left\{ K(\vec{p}_k) + e \cdot W_k(\vec{r}_1,..,\vec{r}_{N(t)},t) - \frac{1}{2} \sum_{\substack{j=1 \\ j\neq k}}^{N(t)} e \cdot V(\vec{r}_k,\vec{r}_j) \right\}, \quad (10)$$

where the term $W_k(\vec{r}_1,.,\vec{r}_k,.,\vec{r}_{N(t)})$ is a particular solution of the following Poisson equation:

$$\nabla^2_{\vec{r}_k}\left(\varepsilon \cdot W_k\left(\vec{r}_1,..,\vec{r}_{N(t)}\right)\right) = \rho_k\left(\vec{r}_1,..,\vec{r}_{N(t)}\right) . \tag{11}$$

The term $\rho_k\left(\vec{r}_1,..,\vec{r}_{N(t)}\right)$ in (11) depends on the position of the first $N(t)$ electrons, i.e.

$$\rho_k\left(\vec{r}_1,.,\vec{r}_k,.,\vec{r}_{N(t)}\right) = \sum_{\substack{j=1 \\ j\neq k}}^{N(t)} e\cdot\delta\left(\vec{r}_k-\vec{r}_j\right), \tag{12}$$

however (12) is independent of the position of the external particles because they only affect the boundary conditions of (11). Let us notice that there are still terms, $V(\vec{r}_k,\vec{r}_j)$, in (10) that are not computed from the Poisson equations in (11), but from (3). If we compare expressions (9) and (10), the term $W_k(\vec{r}_1,..,\vec{r}_{N(t)},t)$ can be rewritten as:

$$W_k(\vec{r}_1,..,\vec{r}_{N(t)},t) = \sum_{\substack{j=1 \\ j\neq k}}^{N(t)} V(\vec{r}_k,\vec{r}_j) + \sum_{i=N(t)+1}^{M} V(\vec{r}_k,\vec{r}_i) \tag{13}$$

The dependence of $W_k(\vec{r}_1,..,\vec{r}_{N(t)},t)$ on the positions of the external particles is explicitly written in the last sum in (13), while in (11) this dependence is hidden in the boundary conditions of $W_k(\vec{r}_1,.,\vec{r}_k,.,\vec{r}_{N(t)})$ on the surface $S = \left\{S^1,S^2,...,S^6\right\}$. In fact, the boundary conditions are a delicate issue that we will discuss in the next section 3.

2.2 Comparison between the many-particle and the standard single-particle Monte Carlo

In this sub-section we emphasize the important differences appearing between the standard MC solution of the BTE, i.e. a time-dependent mean-field algorithm, and our time-dependent many-particle algorithm, i.e. a generalization of the previous single-particle formulation. With this aim in mind, let us first introduce the mean-field version of expression (10).

As described in the introduction of this chapter, the mean-field approximation provides a single average potential for computing the dynamics of all electrons. This average potential, that we label here with the suffix "mean", $\bar{W}_{mean}(\vec{r},t)$, is still capable of preserving most of the collective effects of the Coulomb interaction. The term $\bar{W}_{mean}(\vec{r},t)$ is computed by taking into account all charges inside the volume Ω. However, since one particle can not "feel" its own charge, $\bar{W}_{mean}(\vec{r},t)$ can be interpreted as the electrostatic potential "seen" by an additional probe charge whose position is $\vec{r}$, i.e.

$$\bar{W}_{mean}(\vec{r},t) = \bar{W}_{M+1}(\vec{r}_1[t],..,\vec{r}_{N(t)}[t],\vec{r}), \tag{14}$$

where $\bar{W}_{mean}(\vec{r},t)$ is a solution of a unique 3D-Poisson equation:

$$\nabla^2_{\vec{r}}\bar{W}_{mean}(\vec{r},t) = \bar{\rho}_{mean}\left(\vec{r},t\right), \tag{15}$$

and the charge density is defined as:

$$\bar{\rho}_{mean}\left(\vec{r},t\right)=\sum_{j=1}^{N(t)}q_j\delta\left(\vec{r}-\vec{r}_j[t]\right), \tag{16}$$

Now, it can be shown that the error of the time-dependent mean-field approximation, $Error_k\left(\vec{r},t\right)=\bar{W}_{mean}\left(\vec{r},t\right)-W_k\left(\vec{r},t\right)$, is (Albareda, Suñé & Oriols, 2009):

$$Error_k\left(\vec{r},t\right)=\frac{1}{N(t)}\sum_{j=1}^{N(t)}\left\{\left(\bar{W}_j\left(\vec{r},t\right)-\bar{W}_k\left(\vec{r},t\right)\right)+V(\vec{r},\vec{r}_j[t])\right\}=V(\vec{r},\vec{r}_k[t]), \tag{17}$$

Expression (17) shows that $Error_k\left(\vec{r},t\right)\rightarrow\infty$, when $\vec{r}\rightarrow\vec{r}_k[t]$. The above mean-field approximation implies that the potential "felt" by the k-particle at $\vec{r}\rightarrow\vec{r}_k[t]$ is its own potential profile. In fact, from a numerical point of view, the use of the mean-field approximation is not so bad. For example, classical simulators uses 3D meshes with cell sizes of a few nanometers, $DX\approx DY\approx DZ\gg 10\ nm$. Then, the error of the mean-field approximation is smaller than the technical error (i.e. mesh error) due to the finite size of the cells. The long range Coulomb interaction is well captured with the mean-field approximation, while this approximation is a really bad strategy to capture the short range Coulomb interaction. Finally, let us remark another important point about the mean-field approximation. Looking to the final expression (17), rewritten here as $W_k\left(\vec{r},t\right)=\bar{W}_{mean}\left(\vec{r},t\right)-V(\vec{r},\vec{r}_k[t])$, it seems that $W_k\left(\vec{r},t\right)$ can be computed from a unique mean-field solution of the Poisson equation $\bar{W}_{mean}\left(\vec{r},t\right)$ when subtracting the appropriate two-particle potential $V(\vec{r},\vec{r}_k[t])$. However, such an strategy is not as general as our procedure because it requires an analytical expression for the two-particle Coulomb interaction $V(\vec{r},\vec{r}_k[t])$. The analytical expression of $V(\vec{r},\vec{r}_k[t])$ written in expression (3) is only valid for scenarios with homogenous permittivity. On the contrary, our procedure with $N(t)$ electrostatic potentials computed from $N(t)$ different Poisson equations in a limited 3D volume Ω can be applied inside general scenarios with spatial dependent permittivity.

2.2.1 Simulation of a two-electron system

In order to clarify the above discussion, let us consider one electron (labeled as 1-electron) injected from the source surface, S_4, at an arbitrary position (see Fig. 2). A second electron is injected from the drain surface, S_1 (see Fig. 2). A battery provides an external voltage equal to zero at the drain and source surface. A 3D cubic system with a volume of $\Omega=(20\,nm)^3$ is considered as the active device region. We consider Silicon parameters for the numerical simulation. Within the mean-field approximation only the potential profile $\bar{W}_{mean}(\vec{r},t)$ is calculated for the two-electron system using expressions (14)-(16). Then, we realize from figure 3 that each electron can be reflected by an artificial alteration of the potential profile related to its own charge. In figures 4 and 5 we have plotted the energy potential profile "seen" by the 1-electron, $\bar{W}_1(\vec{r}_1,t)$, and by the 2-electron, $\bar{W}_2(\vec{r}_2,t)$, using the many-particle algorithm described in expressions (25)-(28). Electrons are not longer affected by their own charge. We clearly see that, within the mean-field approximation, electrons could even be unable to overcome the large potential barrier that appears at their own position (due to their own charge). In addition, these simple results confirm that the mean-field error is equal to expression (17), i.e. the error of the mean-field potential profile at each position of the active region is $Error_k\left(\vec{r},t\right)=V(\vec{r},\vec{r}_k\left[t\right])$.

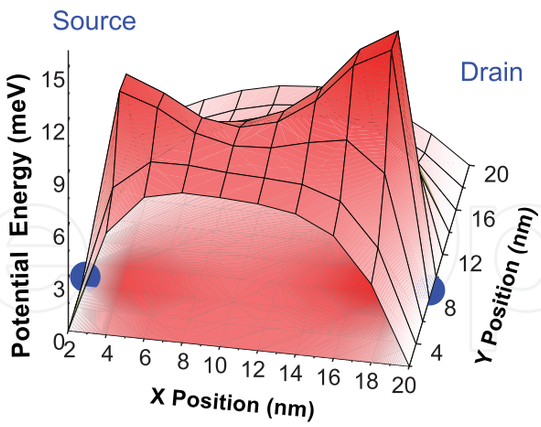

Fig. 3. Potential energy profile $\bar{W}_{mean}(\vec{r},t)$ computed with a 3D Poison solver using the classical "mean-field" approximation on the plane X-Y of the active region $\Omega = (20\,nm)^3$ at z=6nm at 0.4 fs. The solid points are electron positions. Reprinted with permission from G. Albareda et al., Phys. Rev. B. 79, 075315 (2009). ©Copyright 2009, American Physical Society.

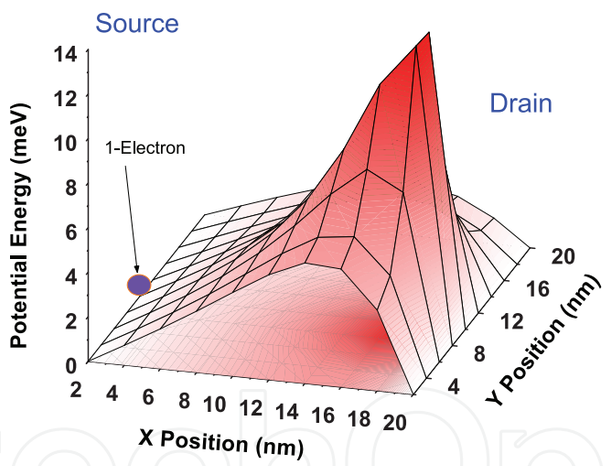

Fig. 4. Potential energy profile of the 1-electron, $\bar{W}_1(\vec{r}_1,t)$, with the "many-electron" algorithm in the plane X-Y of the active region $\Omega = (20\,nm)^3$ at z=6nm at 0.4 fs. The solid point is the 1-electron position. Reprinted with permission from G. Albareda et al., Phys. Rev. B. 79, 075315 (2009). ©Copyright 2009, American Physical Society.

Finally, a discussion about the role of the spatial mesh used for the numerical solution of the Poisson equation is relevant. For an electron device with a length of hundreds of nanometers, we need a mesh of the 3D active region with spatial step $DX \sim DY \sim DZ > 10\,nm$ to deal with no more than one thousand nodes in the numerical solution of the Poisson equation. This computational limitation in the resolution of the potential is present either when solving the mean-field or the many-electron algorithm. With such spatial resolution, the short-range interaction is missing in both procedures because two electrons inside the same spatial cell will

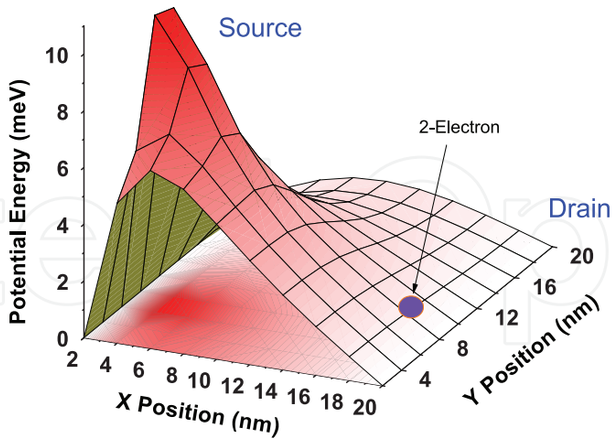

Fig. 5. Potential energy profile of the 2-electron, $\bar{W}_2(\vec{r}_2, t)$, with the "many-electron" algorithm in the plane X-Y of the active region $\Omega = (20\,nm)^3$ at z=6nm at 0.4 fs. The solid point is the 1-electron position. Reprinted with permission from G. Albareda et al., Phys. Rev. B. 79, 075315 (2009). ©Copyright 2009, American Physical Society.

not repel each other. In addition, the error between both procedures, $Error_k\,(\vec{r}, t) = V(\vec{r}, \vec{r}\,[t]_k)$, is reduced because the numerical Coulomb potential profile is smoothed due to the low resolution (i.e. the diameter of the region where $V(\vec{r}, \vec{r}\,[t]_k)$ has a strong influence is shorter than the cell dimensions). Therefore, we obtain roughly identical results with both schemes. On the other hand, for better mesh resolutions ($DX = DY = DZ = 2\,nm$) associated to smaller devices, the differences between both treatments increase due to the important spurious auto-reflection effect found in the mean-field trajectory. In summary, when the spatial cells are large, the mean-field and the many-electron schemes correctly model the long-range Coulomb interaction, but both neglect the short-range component. On the contrary, with smaller spatial steps $DX \sim DY \sim DZ < 5\,nm$, the many-electron resolution takes into account long- and short- range Coulomb interaction correctly, whereas the description of the short-range component within the mean-field approximation is completely incorrect (i.e. electrons are repelled by themselves). In other words, when $DX, DY, DZ \rightarrow 0$ the mesh error in our many-electron algorithm reduces to zero, while the error in the mean-field approach tends to infinite, $Error_k\,(\vec{r}, t) \rightarrow \infty$.

3. Boundary conditions for the many-particle open system Hamiltonian

Let us now move back to the expressions defining our transport problem, i.e. (10), (11) and (12). In order to self-consistently solve electron dynamics in our open system, we need the solutions of the Poisson equations (11). In this regard, the boundary conditions of the $N(t)$ terms $W_k(\vec{r}_1, ., \vec{r}_k, ., \vec{r}_{N(t)})$ in (13) must be specified on the border surfaces $S = \{S^1, S^2, ..., S^6\}$ of figure 2. Such boundary conditions will provide valuable information on the electrostatic effect that the electrons plus the impurities outside have on the electrons inside Ω.
In practical situations, the volume Ω describes the active region of some kind of electron device (a MOSFET for instance). In order to discuss our boundary conditions algorithm, we

assume here a two-terminal device (source and drain)[3]. This means that only two, S^1 and S^4 , of the six border surfaces $S = \{S^1, S^2, ..., S^6\}$ are really opened to the flow of carriers (see figure 6). These opened surfaces represent a complicate problem of boundary conditions that will be discussed in detail in this section (see also Ref. Albareda, López, Cartoixà, Suñé & Oriols, 2010)[4].

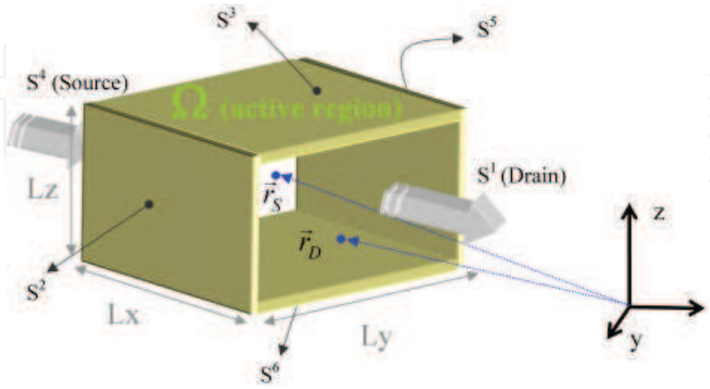

Fig. 6. Schematic representation of the volume $\Omega = Lx \cdot Ly \cdot Lz$ representing a two terminal device. Only S^1 and S^4, corresponding to the drain and source surfaces respectively, are opened to electron flow. On the rest of surfaces standard Neumann boundary conditions are assumed.

3.1 On the importance of boundary conditions

In order to correctly model the DC and/or AC conductance of nanoscale systems, one has to assure the accomplishment of "overall charge neutrality" and "current conservation" (Blanter & Büttiker, 2000; Landauer, 1992). As we have mentioned, the implementation of such requirements into modern nanoscale electron simulators demands some kind of reasonable approximation for the Coulomb interaction.

In general, modern electron transport simulators do include reasonable approximations for the coulomb interactions that can guarantee the accomplishment of the "overall charge neutrality" requirement. In addition, those simulators that are developed within a time-dependent or frequency-dependent framework can also assure the "current conservation" requirement. However, the treatment of many-particle electron transport can only be applied to a very limited number of degrees of freedom. In fact, due to computational restrictions, a small simulation box is a mandatory requirement in modern MC simulators. This restriction implies that either very short leads (with screening length of few Armstrongs) are included into the small simulation box, or the leads are directly excluded from the simulation box. The first solution is only acceptable for metallic leads (Brandbyge et al., 2002;

[3] In any case, the boundary conditions can be straightforwardly adapted to multi-terminal systems with an arbitrary number of "opened" borders.

[4] On the "closed" non-metallic surfaces [5], Neumann boundary conditions are used with the educated guess that the component of the electric field normal to that surfaces is zero. The continuity of the displacement vector normal to surfaces justifies this assumption on "closed" (i.e. no electrons traversing the surfaces) boundaries when the relative permittivity inside is much higher than the corresponding value outside. On "open" metallic surfaces, we use a many-particle version of the standard Dirichlet boundary conditions (Albareda, Suñé & Oriols, 2009)

Taylor et al., 2001) close to equilibrium, but it becomes inappropriate in general scenarios ranging from highly doped poly-silicon leads (with screening length of few nanometres) till modern juntionless devices (Collinge, 2010). In far-from equilibrium conditions (i.e. high bias conditions), the standard screening lengths have to be complemented by an additional depletion length in the leads. The second solution (neglecting the leads) implies serious difficulties for the achievement of "overall charge neutrality". In any case, a possible inaccuracy in the computation of the "overall charge neutrality" affects our ability to treat the time-dependent Coulomb correlation among electrons and, therefore, the requirement of "current conservation". In conclusion, due to computational difficulties, modern electron transport simulators have to be implemented in small simulation boxes that imply important difficulties for providing accurate simulations of the DC or AC conductances of nanoscale devices.

In principle, the problem of excluding the leads from the simulation box, while retaining the lead-sample Coulomb correlation, can be solvable by providing adequate boundary conditions on each of the "opened" borders of the simulation box. However, such boundary conditions are not easily predictable. The standard boundary conditions found in the literature for nanoscale electron device simulators are based on specifying two conditions in each of the borders of the simulation box:

(Border-potential-BC).- The value of the scalar potential (or electric field) at the borders of the simulation box has to be specified. This condition is a direct consequence of the uniqueness theorem for the Poisson equation (Javid & Brown, 1963) which tells that such condition are enough to completely specify the solution of Poisson equation, when the charge inside the simulation box is perfectly determined (the reason for discarding the electromagnetic vector potential in nansocale systems is discussed in Ref. Albareda, López, Cartoixà, Suñé & Oriols, 2010).

(Border-charge-BC).- Contrarily to what is needed for the uniqueness solution of the Poisson equation, the charge density inside the simulation box is uncertain because it depends on the electron injected from the borders of the simulation box. Therefore, any boundary condition algorithm has to include the information on the charge in the borders as an additional condition. In many cases, the electron injected on the borders depends, somehow, on the scalar potential there determined by the "Border-potential-BC" (and a fixed electrochemical potential). Therefore, a coupled system of boundary conditions appears.

Educated guesses for both boundary conditions ("Border-potential-BC" and "Border-charge-BC") are present in the literature when describing nanoscale electron devices with simulation boxes large enough to include the leads. However, such boundary conditions are not applicable for small simulation boxes that exclude the leads. Here, we present a novel self-consistent and time-dependent definition of the boundary conditions for small simulation boxes (excluding most of the leads) that is able to capture the lead-sample Coulomb correlations (Albareda, López, Cartoixà, Suñé & Oriols, 2010).

3.2 Time-dependent boundary-conditions at the borders of the sample for overall charge neutrality

As explained in the previous paragraphs, all boundary condition of electrons transport simulators are based on specifying the value of the scalar potential (or the electric field) in the

borders and the charge density there. Therefore, according to the labels of figure 7, we have to specify the values $V_S(t)$ and $V_D(t)$ for the "Border-potential-BC", and $\rho_S(t)$ and $\rho_S(t)$ for the "Border-charge-BC". Unfortunately, it is very difficult to provide an educated guess of the

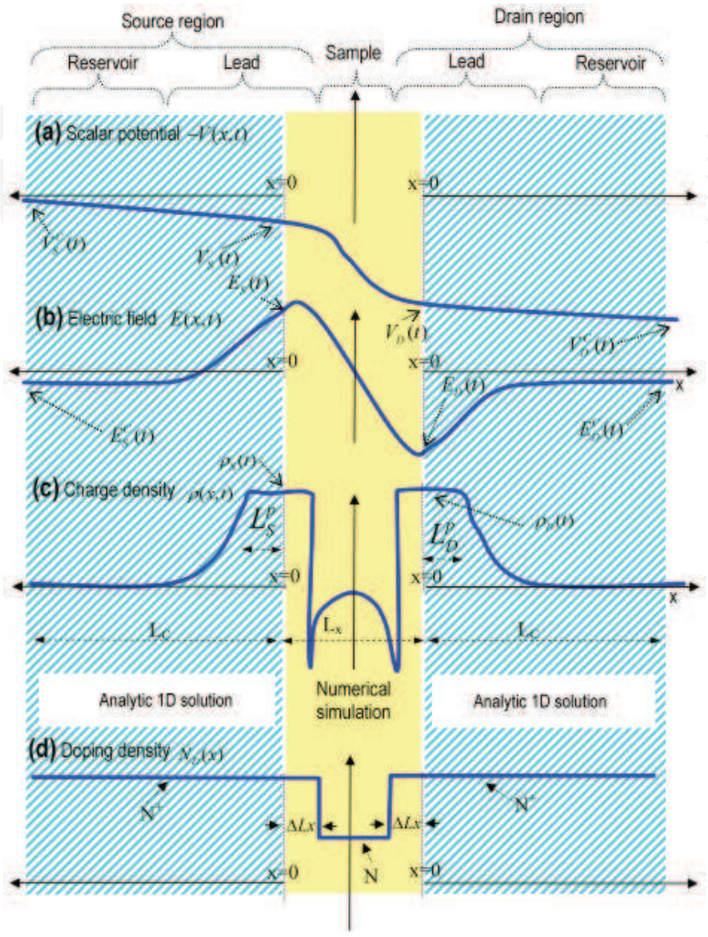

Fig. 7. Schematic description of the different parts of the electron device. In Ref. Albareda, López, Cartoixà, Suñé & Oriols, 2010, an analytical parametric 1D solution is deduced for the (blue) dashed region, while a numerical 3D solution is obtained in the (yellow) solid central region defined as the simulation box. Subsets refer to schematic representation of the (a) scalar potential, (b) electric field, (c) total charge density and (d) doping density. Reprinted with permission from G. Albareda et al., Phys. Rev. B. 79, 075315 (2009). ©Copyright 2009, American Physical Society.

scalar potential, the electric field or the charge density on the borders of a small simulation box that excludes the leads. For large simulation boxes, one can assume a known value of the electrochemical potential (deep inside the reservoir) that controls the electron injection. However, close to the active region, where there exists a far from equilibrium momentum distribution, the prediction of any value of the electrochemical potential is quiet inappropriate. From the results in Ref. Albareda, López, Cartoixà, Suñé & Oriols, 2010, we are able to translate the "Border-potential-BC" and "Border-charge-BC" discussed in section 3.1, for the borders of a small simulation box into simpler conditions deep inside the reservoirs. This is

the key point of our boundary conditions algorithm. In particular, the two new boundary conditions that we will impose at the limits of the simulation box, $x = \mp L_C$ are (see Fig. 7):

"Deep-drift-BC": We assume that the inelastic scattering mechanisms at, both, the source $x \leq -L_C$ and the drain $x \geq L_C$ reservoirs provides a non-equilibrium position-independent "thermal" distribution of electrons there (it is implicitly assumed that the contact length L_C is large enough and the temperature Θ high enough so that inelastic scattering is relevant there). Such position-independent electron distribution is consistent with the "local" charge neutrality that implies a uniform electric field there. According to the Drude's model, the electric fields there tend both to $E^C_{S/D}(t) \rightarrow E^{drift}_{S/D}(t)$ [see expressions (11) and (12) of Ref. Albareda, López, Cartoixà, Suñé & Oriols, 2010].

"Deep-potentail-BC": We assume that electro-chemical potentials can be defined for the "thermal" distribution deep inside both reservoirs. As a consequence of the previous position-independent electron distribution deep inside the reservoirs, we can assume that the energy separation between such electro-chemical potential level and the bottom of the conduction band, in the drain and source reservoirs (at $x = \mp L_C$) are equal. Therefore, the energy separation between the bottoms of the conduction bands at both reservoirs (which coincides with the separation of the electrochemical potentials) is equal to the difference of the external voltages. Thus, $V^C_S(t) = 0$ and $V^C_D(t) = V_{external}(t)$.

These two conditions, "Deep-drift-BC" and "Deep-potential-BC" are quite reasonable deep inside the reservoirs. In fact, it can be shown that the numerical MC solution of the non-equilibrium BTE in a large simulation box provides exactly these results in the reservoirs (see Ref. Albareda, López, Cartoixà, Suñé & Oriols, 2010).

In order to translate the above "deep" boundary conditions into practical considerations on the simulation box borders, our algorithm couples the charge density, the electric field and the scalar potential to the injection model by taking into account the electrostatic interaction among the electrons within the active region and those in the leads (see Ref. Albareda, López, Cartoixà, Suñé & Oriols, 2010). Following this strategy, the amount of charge on the whole circuit can be set to zero, and thus "overall charge neutrality" and "current conservation" requirements are accomplished. The main approximation used to obtain the previous results is Drude's law. Thus, our time-dependent boundary condition algorithm is only valid for frequencies below the inverse of the average electron scattering time (see Ref. Albareda, López, Cartoixà, Suñé & Oriols, 2010). In good reservoirs such frequencies are much higher than the THz range, which is high enough for most practical electronic applications.

The formulation of the previous boundary conditions, however, corresponds to a single-particle system. That is, we assume that all electrons are subjected to the same boundary conditions. Again, this is a simplification of the real many-particle problem. As we have shown in the previous section (see equations (10), (11) and (11)), every single electron "sees" its own electrostatic potential, electric field and charge distribution. Consequently, each electron should see its own boundary conditions. In the next section we extent these boundary conditions to a many-particle ones.

3.3 Extension of the boundary conditions to many-particle Hamiltonians

In the previous subsection we have presented a unique set of time-dependent boundary conditions for all electrons to account for overall charge neutrality and current conservation. Here we extent such results to a many-particle level where each electron has its own boundary conditions. Let us recall, that we are looking for solutions of the $N(t)$ Poisson equations (11). Thus, we need to specify $N(t)$ boundary conditions on the two opened border surfaces S^1 and S^4 (see figure 6) for the $N(t)$ terms $W_k(\vec{r}_1,.,\vec{r}_k,.,\vec{r}_{N(t)})$.

In order to provide a clear notation for discussing the boundary conditions of $W_k(\vec{r}_1,...,\vec{r}_k,...,\vec{r}_{N(t)})$, we distinguish between the "source" vectors $\{\vec{r}_1,...,\vec{r}_{k-1},\vec{r}_{k+1},...,\vec{r}_{N(t)}\}$ and the additional "observation" vector $\vec{r}$ that runs over all space (Javid & Brown, 1963). In particular, the electrostatic potential that appears in the Hamiltonian (9) is defined as the value of the potential $W_k(\vec{r}_1,...,\vec{r}_{k-1},\vec{r},\vec{r}_{k+1},...,\vec{r}_{N(t)},t)$ at the particular position $\vec{r}=\vec{r}_k$:

$$W_k(\vec{r}_1,..\vec{r}_{k-1},\vec{r}_k,\vec{r}_{k+1}.,\vec{r}_{N(t)},t) = W_k(\vec{r}_1,..\vec{r}_{k-1},\vec{r},\vec{r}_{k+1}.,\vec{r}_{N(t)},t)\Big|_{\vec{r}=\vec{r}_k} \tag{18}$$

Our goal is to find an educated guess for all the $N(t)$ terms $W_k(\vec{r}_1,..\vec{r}_{k-1},\vec{r},\vec{r}_{k+1}.,\vec{r}_{N(t)},t)$ at all "observation" points $\vec{r}=\vec{r}_S$ and $\vec{r}=\vec{r}_D$ on the surfaces S^1 and S^4. The information of such boundary conditions comes from the value of the total voltage (due to internal and external electrons) at position $\vec{r}_{S/D}$ and time t, that can be defined as the electrostatic potential associated to an additional probe charge q_{M+1} situated on that boundary, $\vec{r}_{S/D}\equiv\vec{r}_{M+1}\in S^{4/1}$. This potential can be then identified with the voltages $V_{S/D}(t)$ defined in the previous subsection (see fig. 8), i.e.

$$V_{S/D}(t)\equiv\sum_{j=1}^{M}V(\vec{r}_{M+1},\vec{r}_j)\Big|_{\vec{r}_{M+1}=\vec{r}_{S/D}} \tag{19}$$

where the expected restriction $j\neq M+1$ is hidden in the limit of the sum. Once the relationship (19) is established, we can easily define the boundary conditions of any of the $N(t)$ electrostatic potential $W_k\left(\vec{r}_1,.,\vec{r},.,\vec{r}_{N(t)}\right)$ from the function $V_{S/D}(t)$. In particular, from (13), we know that:

$$W_k(\vec{r}_1,..\vec{r}_{k-1},\vec{r},\vec{r}_{k+1}.,\vec{r}_{N(t)},t)\Big|_{\vec{r}=\vec{r}_{S/D}} = \sum_{\substack{j=1\\ j\neq k}}^{M}V(\vec{r}_{S/D},\vec{r}_j) = V_{S/D}(t)-V(\vec{r}_{S/D},\vec{r}_k) \quad ;\ l=1,...,6 \tag{20}$$

where $V(\vec{r}_{S/D},\vec{r}_k)$ is defined according to (3).

4. Monte Carlo solution of the many-particle open system Hamiltonian

Once we have introduced the many-particle open system Hamiltonian and its boundary conditions, we are ready to solve the electron transport problem. The classical description of the particle dynamics subjected to the many-particle Hamiltonian (10) can be computed by using the well-known Hamilton equations. In particular, we can obtain the (Newton like)

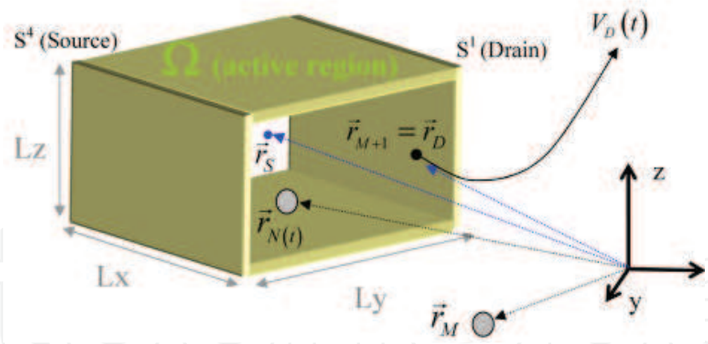

Fig. 8. The electrostatic potential $V_D(t)$ (due to internal and external electrons) measured on the surface S^1 at position $\vec{r}_D$ and time t by an additional probe charge q_{M+1} situated on the boundary $\vec{r}_D \equiv \vec{r}_{M+1} \in S^1$.

description of the classical trajectory $\vec{r}_i[t]$ in the real space through:

$$\frac{d\vec{p}_i[t]}{dt} = \left[-\nabla_{\vec{r}_i} H(\vec{r}_1,..,\vec{r}_{N(t)},\vec{p}_1,..,\vec{p}_{N(t)},t)\right]_{\vec{r}_1=\vec{r}_1[t],..,\vec{p}_{N(t)}=\vec{p}_{N(t)}[t]}, \tag{21a}$$

$$\frac{d\vec{r}_i[t]}{dt} = \left[\nabla_{\vec{p}_i} H(\vec{r}_1,..,\vec{r}_{N(t)},\vec{p}_1,..,\vec{p}_{N(t)},t)\right]_{\vec{r}_1=\vec{r}_1[t],..,\vec{p}_{N(t)}=\vec{p}_{N(t)}[t]}. \tag{21b}$$

For the many-particle Hamiltonian studied here, expression (21b) gives the trivial result $m \cdot \vec{v}_i[t] = \vec{p}_i[t]$, while the evaluation of expression (21a) requires a more detailed development. We know that the $\vec{r}_i$-gradient of the exact many-particle Hamiltonian (10) can be written as:

$$\left[\nabla_{\vec{r}_i} H\right]_{\vec{R}=\vec{R}[t]} = \left[\nabla_{\vec{r}_i} \sum_{k=1}^{N(t)} \left\{ e \cdot W_k(\vec{r}_1,..,\vec{r}_{N(t)},t) - \frac{1}{2} \sum_{\substack{j=1 \\ j\neq k}}^{N(t)} e \cdot V(\vec{r}_k,\vec{r}_j) \right\}\right]_{\vec{R}=\vec{R}[t]}. \tag{22}$$

We define the multi-dimensional vector $\vec{R} = \left(\vec{r}_1,...,\vec{r}_{N(t)}\right)$ to account, in a compact way, for the classical trajectories of $N(t)$ electrons $\vec{R}[t] = \left(\vec{r}_1[t],...,\vec{r}_{N(t)}[t]\right)$. Substituting the definition of $W_k(\vec{r}_1,..,\vec{r}_{N(t)},t)$ of expression (13) into equation (22), we find:

$$\left[\nabla_{\vec{r}_i} H\right]_{\vec{R}=\vec{R}[t]} = \left[\nabla_{\vec{r}_i} \left\{ 2 \sum_{\substack{j=1 \\ j\neq i}}^{N(t)} eV(\vec{r}_j,\vec{r}_i) + \sum_{j=N(t)+1}^{M} eV(\vec{r}_j,\vec{r}_i) \right\} - \nabla_{\vec{r}_i} \sum_{\substack{j=1 \\ j\neq i}}^{N(t)} e \cdot V(\vec{r}_j,\vec{r}_i) \right]_{\vec{R}=\vec{R}[t]}. \tag{23}$$

Now, from expressions (13) and (23), we realize that:

$$\left[\nabla_{\vec{r}_i} H\right]_{\vec{R}=\vec{R}[t]} = \left[\nabla_{\vec{r}_i} W_i(\vec{r}_1,..,\vec{r}_{N(t)})\right]_{\vec{R}=\vec{R}[t]}. \tag{24}$$

Only the term $W_i(\vec{r}_1,..,\vec{r}_{N(t)})$ of the whole Hamiltonian (10) becomes relevant for a classical description of the i-particle. In fact, since we only evaluate a $\vec{r}_i$-gradient, the rest of particle positions can be evaluated at their particular value at time t, i.e. $\vec{r}_k \rightarrow \vec{r}_k[t]$ for all $k \neq i$.

Therefore, we define the single-particle potential $\bar{W}_i(\vec{r}_i,t)$ from the many-particle potential as:

$$\bar{W}_i(\vec{r}_i,t) = W_i(\vec{r}_1[t],..,\vec{r}_{i-1}[t],\vec{r}_i,\vec{r}_{i+1}[t],..,\vec{r}_{N(t)}[t]). \tag{25}$$

We use a "hat" to differentiate the (time-dependent) single-particle electrostatic potential from the many-particle potential. Each i-term of the single-particle electrostatic potential, $\bar{W}_i(\vec{r}_i,t)$, is a solution of one particular 3D-Poisson equation:

$$\nabla^2_{\vec{r}_i}\left(\varepsilon(\vec{r}_i)\cdot\bar{W}_i\left(\vec{r}_i,t\right)\right) = \bar{\rho}_i\left(\vec{r}_i,t\right), \tag{26}$$

where the single-particle charge density is defined as:

$$\bar{\rho}_i\left(\vec{r}_i,t\right) = \sum_{\substack{j=1\\ j\neq i}}^{N(t)} e\dot{\delta}\left(\vec{r}_i - \vec{r}_j[t]\right), \tag{27}$$

and the boundary conditions are adapted here as:

$$\bar{W}_i\left(\vec{r}_i,t\right)\big|_{\vec{r}_i=\vec{r}_{S/D}} = V_{S/D}(t) - V\left(\vec{r}_{S/D},\vec{r}_i[t]\right). \tag{28}$$

Let us remind that expressions (25), (26) and (27) together with the boundary conditions in (28), provide an exact treatment of the many-particle correlations in classical scenarios. The $N(t)$ Newton equations are coupled by $N(t)$ Poisson equations. Therefore, the many-particle Hamiltonian of (10) can be written exactly (without mean-field approximation) as:

$$H(\vec{r}_1,..,\vec{r}_{N(t)},\vec{p}_1,..,\vec{p}_{N(t)},t) = \sum_{k=1}^{N(t)}\left\{K(\vec{p}_k) + e\cdot\bar{W}_k(\vec{r}_k,t)\right\}. \tag{29}$$

It is important to recall here that, although electron dynamics within our open system is *deterministically* described by the many-particle Hamiltonian (10) supplied with the Hamilton equations (21), our simulations will be subject to an *stochastic injection* of electrons describing how (i.e. in which position, time and momentum) electrons enter the simulated region. Indeed, our approach to electron transport ultimately constitutes an statistical problem. Due to computational limitations, we have been forced to reduce the degrees of freedom of our system. Since we can only describe a very reduced number of variables in a very reduced region of space (an open system representing the active region of an electron device), we are obliged to deal with an essentially uncertain environment. The injection process, is then the responsible of coupling an statistical *external* environment to our "deterministic" simulation box, and thus, it is also the main responsible of converting the information that we have on the dynamics occurring inside the simulation region into something statistical (Albareda, López, Cartoixà, Suñé & Oriols, 2010). It is in this regard that we can classify our approach to electron transport as a MC technique. Nonetheless, as we have already announced, our many-electron method applied to semiclassical devices cannot be considered a solution of the BTE because the latter is developed at a classical mean-field level. The term $\bar{W}_k(\vec{r}_k,t)$ in the Hamiltonian of expression (29) means that each particle "sees" its own electrostatic potential which is different to that of the others. Apart from the scattering rates, this is the fundamental difference between our "many-electron" method applied to classical transport and the standard MC solution of the BTE method for electron devices.

Let us just mention here that the previous algorithm developed to describe classical electron transport at a many-particle level can be easily generalized to quantum systems by means of an original formalism based on quantum trajectories (Oriols, 2007; Oriols & Mompart, 2011). In particular, recent efforts have made it possible to demonstrate the viability to develop a quantum trajectory-based approach to electron transport with many-particle correlations (Albareda, 2010; Albareda, López, Cartoixà, Suñé & Oriols, 2010; Albareda, Suñé & Oriols, 2009). We have named this simulator BITLLES.

5. Numerical example: Many-particle transport in the channel of quantum wire DG-FETs with charged atomistic impurities

Up to now we have been focused mainly on the theoretical aspects of our MC approach to electron transport. Sections 2, 3 and 4 constitute the keystone pieces for the development of a versatile simulation tool capable of describing semi-classical electron transport including Coulomb correlations at a many-particle level. The aim of this section is to present an example of the capabilities of such a simulator to predict certain relevant aspects of future nanoscale electron devices. In particular, we want to highlight the importance of accurately accounting for (time-dependent) Coulomb correlations among (transport) electrons in the analysis of discrete doping induced fluctuations.

Differences in number and position of dopant atoms in sub-10nm channel devices will produce important variations on the devices' microscopic behavior, and consequently, the variability of macroscopic parameters such as drive current or threshold voltage will increase. This particular phenomenon is known as discrete dopant induced fluctuations, and constitutes one of the most reported causes of variations from sample to sample in electron devices characteristics (coming from the atomistic nature of mater). We study here the effect of single ionized dopants on the performance of a quantum wire double-gate FET (QWDG-FET), mainly when its lateral dimensions approach the effective cross section of the charged impurities. We find that neglecting the (time-dependent) Coulomb correlations among (transport) electrons can lead to misleading predictions of devices behavior (Albareda, Saura, Oriols & Suñé, 2010).

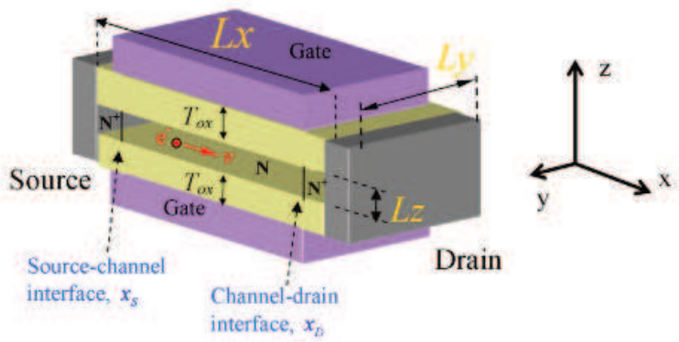

Fig. 9. Schematic representation of the quantum wire double gate FET.

5.1 Device Characteristics and Simulation Details

The structure of the simulated QWDG-FET is described in figure 9. Two highly N doped Si contacts ($N^+ = 2 \cdot 10^{19}\, cm^{-3}$) are connected to an intrinsic Si channel with lateral dimensions

$L_y = 5nm$ and $L_z = 2nm$. Such dimensions originate quantum confinement in the lateral directions (a quantum wire), not only reducing the degrees of freedom of the system but also inducing volume inversion within the channel (Balestra et al., 1987). In this regard, the electrostatic blockade generated by the ionized dopants is expected to be favored when impurities are distributed mainly in the center of the channel cross section. At the same time, the length of the quantum wire is $10nm$. This geometry results in a volume of only $100nm^3$, so that the number of interacting electrons in the channel is of the order of 10. Under such special conditions, the importance of the correlation among electrons is expected to be particularly relevant.

Electron transport in the "x" direction (from source to drain) takes place along a Silicon (100) oriented channel, at room temperature. In particular, the electron mass is taken according to the six equivalent ellipsoidal constant energy valleys of the silicon band structure (Jacoboni & Reggiani, 1983; Oriols et al., 2007). The effective masses of the ellipsoids are $m_l^* = 0.9163\, m_0$ and $m_t^* = 0.1905\, m_0$ with m_0 being the free electron mass (Jacoboni & Reggiani, 1983). As commented above, the lateral dimensions of the Si channel L_z and L_y are both small enough, so that the active region behaves as a 1D system and the energy of an electron in one particular valley is $E = \hbar^2 k_x / (2m_t) + E_{1D}^q$, where $E_{1D}^q = \hbar^2\pi^2 / \left(2m_t L_y^2\right) + \hbar^2\pi^2 / \left(2m_l L_z^2\right)$ represents the minimum energy of the first sub-band, whose value is $E_{1D}^q = 0.182eV$ for $L_z = 2nm$ and $L_y = 5nm$. The energies of the next lowest sub-bands ($E_{1D}^q = 0.418eV$ or $E_{1D}^q = 0.489eV$) are assumed to be high enough to keep a single band simulation sufficiently accurate. Therefore, we use a 3D Poisson solver to deal with the device electrostatics, but a 1D algorithm to describe the velocity of each electron in the "x" direction. Due to the lateral electron confinement, the velocities in "y" and "z" directions are zero[6]. This is an exact result for describing electron confinement in the rectangular structure of figure 9 when the e-e and e-i are not taken into account. The explicit consideration of the effect of e-e and e-i correlations on the electron confinement (energy levels) is an extremely complicated issue within the many-particle strategy developed here, which considers one different scalar potential for each electron. The reader can find more information on the simulation details in Ref. Albareda, Saura, Oriols & Suñé, 2010.

5.2 Analysis of discrete doping induced fluctuations

In order to highlight the importance of taking into account the time-dependent e-e and e-i correlations, we will compare some results with those obtained through a single-particle mean-field approach discussed in Ref. Albareda, Saura, Oriols & Suñé, 2010. In this regard, we will refer to many-particle results to describe the simulation performed with the algorithms that require solving $N(t)$ Poisson equations with $N(t)$ charge densities [expressions (26),(27),(28)] at each time step. Alternatively, we will refer to the time-independent single-particle approximation to the more simplistic (though usual) approach that consists in solving a single time-independent Poisson equation [expressions (A1) and (A2) in Ref. Albareda, Saura, Oriols & Suñé, 2010 for all electrons at each time step of the simulation.

[6] We assume that the electron velocity is equal to zero in the lateral directions where there is energy confinement. This is a reasonable assumption that can be formally justified (see Ref. Oriols, 2007) when the probability presence in that direction does not change with time. The main approximation here is assuming that the time dependence of the wave function involves only one quantized energy in the mentioned direction. We define the geometry of the QWDG-FET to support these approximations.

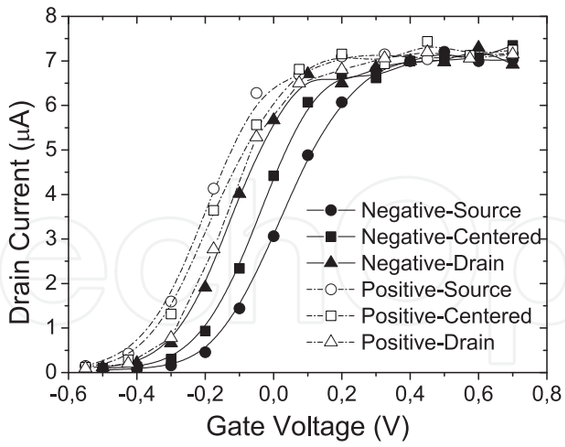

Fig. 10. Average drain current at $V_{Drain} = 1V$ as a function of the gate voltage for positive/negative impurities located at different places along the channel. Reprinted with permission from G. Albareda et al., J. Appl. Phys. 108, 043706 (2010). ©Copyright 2010, American Institute of Physics.

Let us start the discussion with the study of threshold voltage (V_T) fluctuations, a well known effect related to discrete doping induced fluctuations in MOSFETs (Asenov, 1999; Asenov et al., 2003; Gross et al., 2002; Millar et al., 2008; Reid et al., 2009; Vasileska & Ahmed, 2005). We first analyze this phenomenon in the QWDG-FET for both positive and negative impurities. Fig. 10 shows the value of the mean current as a function of the applied gate voltage (transfer characteristic) in the saturation region ($V_{Drain} = 1V$). While negative ions induce a shift of the threshold voltage towards higher values, positively charged impurities shift it down to lower values. The explanation of such a behavior is quite simple. Since the majority carriers are electrons, positive charged impurities introduce a potential well that favors the flow of the current, while negative impurities appear as potential barriers which tend to block the transmission of electrons. A dependence of the saturation threshold voltage on the position of the impurities along the channel can also be observed. As a negative (positive) dopant is displaced from drain to source, the threshold voltage is increased (decreased) in a non-linear way due to an increment of the height (depth) of the induced potential deformation that is less and less masked by the applied drain voltage (Albareda, Saura, Oriols & Suñé, 2010).
Next, we show how negative dopants placed in the channel of a QWDG-FET induce significant changes in the spatial distribution of the current-density across the channel section. We consider the steady state current corresponding to a fixed bias point ($V_{Gate} = 0V$; $V_{Drain} = 0.5V$) and analyze the spatial distribution of the current in the channel cross section. Since we deal with a confined electron system under stationary conditions, the continuity equation reduces to $\vec{\nabla} J_x = 0$ and consequently the spatial distribution of the current-density, J_x, is the same in any section along the transistor channel. In figure 11 we present the current-density distribution when a negative impurity is located at the source-channel interface. As it can be observed, the potential barrier produced by the dopant induces an important deformation of the spatial current density distribution, pushing carriers away from its location. This is a common result to both single- and a many-particle treatment of electron transport. However, differences on the magnitude of the current-density between Fig. 11.a) and Fig.

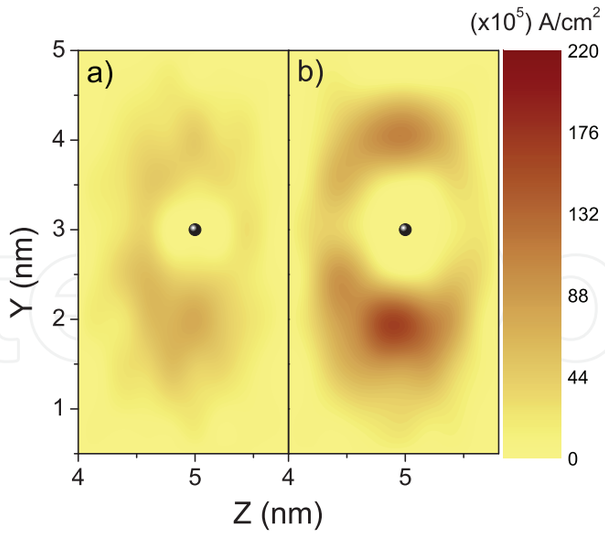

Fig. 11. Current density across the channel section when the negative impurity is placed at the center of the channel length. In a) the results correspond to a many-particle treatment of the system. In b) the results have been computed within a single-particle mean-field approach discussed in Ref. (Albareda, Saura, Oriols & Suñé, 2010). Reprinted with permission from G. Albareda et al., J. Appl. Phys. 108, 043706 (2010). ©Copyright 2010, American Institute of Physics.

11.b) are only attributable to fundamental differences among both treatments. Although from a single-particle point of view, a one-by-one electron energy conservation must be accomplished, many-particle transport implies a much looser restriction on the energy of the carriers.

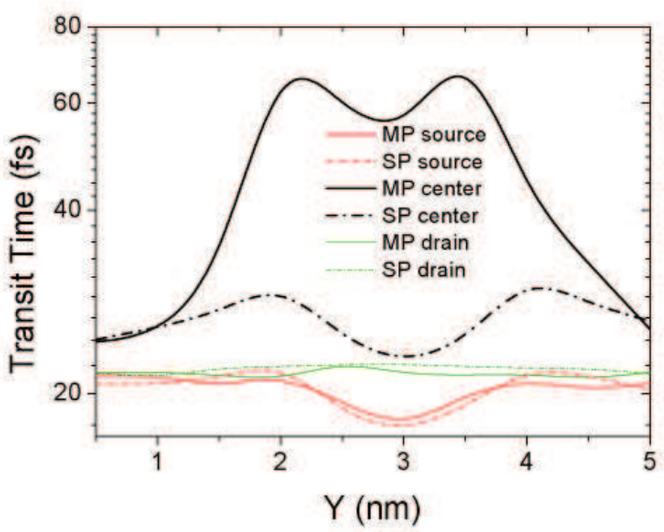

Fig. 12. Spatial distribution of the transit times along the *y* direction (centred in z) when a negatively charged impurity is placed at different places of the channel. Reprinted with permission from G. Albareda et al., J. Appl. Phys. 108, 043706 (2010). ©Copyright 2010, American Institute of Physics.

In figure 12 we represent the distribution of the transit times along the y (centered in z) direction. If all the traversing carriers had the same total energy, one would expect to find the largest transit times concentrated around the impurity location, where the potential barrier is higher (see Fig. 12). Nevertheless, since the injected carriers are energetically spread according to Fermi statistics, only the fastest electrons (the most energetic ones) are able to achieve the drain contact across the top of the barrier. Therefore, a minimum of the transit time is found at the location of the impurity atom. When the dopant is placed at the source-channel interface, the largest transit times appear away from the impurity and the minimum above the dopant becomes absolute. Although both, single- and many-particle simulations give similar overall results in this case, some discrepancies can be appreciated due to an energy exchange among the different regions of the channel. When the impurity is placed in the center of the channel, the transit times increase drastically up to 60 fs. Although the shape of the scalar potential is the responsible of the important increment in both the single-particle and the many-particle transit times results, electron-electron interactions play a crucial role in explaining the important differences between these two treatments. Since the spatial integral of the many-particle averaged transit times along the y and z directions diverges significantly from its single-particle counterpart, it can be inferred that the exchange of energy is produced not only among the electrons crossing the channel but also between them and those being backscattered (Albareda, Saura, Oriols & Suñé, 2010). Indeed, if the energy transfer would only involve electrons crossing the device, their total energy would remain unchanged, and thus their averaged transit time would be identical to that found for the single-particle approach. On the contrary, the mixture of energy exchange among the traversing electrons and among traversing and backscattered electrons give rise to a non conserving averaged transit time.

6. Conclusions

In this chapter we have presented a semi-classical MC approach to electron transport at the nanoscale without assuming any mean-field or perturbative approximation to describe the Coulomb interaction among transport electrons. Sections 2, 3 and 4 constitute the theoretical core of our semi-classical MC approach. In section 2, a many-particle Hamiltonian for $N(t)$ electrons inside an open system has been developed. Departing from the exact Hamiltonian of a whole closed circuit, using a single-band effective mass approximation we are capable of developing a many-particle Hamiltonian (10) constituted by a sum of $N(t)$ electrostatic potentials, $W_k(\vec{r}_1,.,\vec{r}_k,.,\vec{r}_{N(t)})$, solution of $N(t)$ different Poisson equations (11). In section 3, we have presented a novel boundary conditions algorithm capable of describing the Coulomb correlations among electrons inside and outside the open system without significantly increasing the simulated degrees of freedom. In terms of analytical expressions describing the charge density, the electric field and the scalar potential along the leads and reservoirs, we can transfer the assumptions about the boundary conditions at the borders of a small simulation boxes into the simpler specifications of the boundary conditions deep inside the reservoirs. Our boundary conditions algorithm is able to discuss far from equilibrium situations where depletion lengths in the leads have to be added to standard screening. More over, the frequency-dependent correlations included into our boundary conditions algorithm, due to sample-lead Coulomb interaction, allow us to investigate the computation of (zero-frequency and high-frequency) current fluctuations beyond the standard external zero impedance assumption (i.e. most of the computations of current fluctuations in

electron devices assume that the voltage applied in the simulation box is a non-fluctuating quantity). In section 4, we have presented a classical solution of the many-particle open system Hamiltonian supplied with our many-particle boundary conditions. The solution is obtained via a coupled system of Newton-like equations with a different electric field for each particle, and constitutes a many-particle generalization of the MC solution of the semi-classical single-particle Boltzmann distribution. In the last section, our many-particle approach to electron transport has been applied to predict the behavior of some characteristics of a QWDG-FET under the presence of discrete impurities. We have revealed the significant impact of the sign and position of the impurity along the transistor channel on the threshold voltage, but more importantly, a comparison with more standard simulations which assume a time-independent mean-field approximation has allowed us to highlight the importance of an accurate treatment of the e-e interactions in the study of discrete doping induced fluctuations in nanometer scale devices. Finally, let us emphasize that many efforts are being devoted in the literature to improve the treatment of electron (and electron-atom) correlations on the description of the band structure of nanoscale devices (i.e. the ground-state at equilibrium conditions). Contrarily, in this work we open a new path to study the effects of electron (and electron-impurity) correlations in the current measured in nanoscale electron devices under (applied bias) far from equilibrium conditions.
Finally, let us mention that the presented technique can be also extended to describe quantum transport by means of bohmian trajectories (Alarcon & Oriols, 2009; Albareda, 2010; Albareda, López, Cartoixà, Suñé & Oriols, 2010; Albareda, Suñé & Oriols, 2009; Oriols, 2007). In this regard, a versatile (classical and quantum) many-particle approach to electron transport, called BITLLES, capable of reproducing DC, AC and noise performance in quantum scenarios has been already developed (Albareda, 2010; Oriols & Mompart, 2011).

Acknowledgments

We would like to thank doctors D. Pardo, T. González and J. Mateos from Universidad de Salamanca. The MC method presented in this work is an evolution of their technique towards simulations tools with a full treatment of Coulomb correlations. This work has been partially supported by the Ministerio de Ciencia e Innovación under Project No. TEC2009-06986 and by the DURSI of the Generalitat de Catalunya under Contract No. 2009SGR783.

7. References

Alarcon, A. & Oriols, X. (2009). Computation of quantum electron transport with local current conservation using quantum trajectories, *Journal of Statistical Mechanics: Theory and Experiment* 2009: P01051.

Albareda, G. (2010). *Classical and Quantum Trajectory-based Approaches to Electron Transport with full Coulomb Correlations*, PhD thesis, Universitat Autònoma de Barcelona.

Albareda, G., Jiménez, D. & Oriols, X. (2009). Intrinsic noise in aggressively scaled field-effect transistors, *Journal of Statistical Mechanics* 2009: P01044.

Albareda, G., López, H., Cartoixà, X., Suñé, J. & Oriols, X. (2010). Time-dependent boundary conditions with lead-sample coulomb correlations: Application to classical and quantum nanoscale electron device simulators, *Physical Review B* 82(8): 085301.

Albareda, G., Saura, X., Oriols, X. & Suñé, J. (2010). Many-particle transport in the channel of quantum wire double-gate field-effect transistors with charged atomistic impurities, *Journal of Applied Physics* 108(4): 043706.

Albareda, G., Suñé, J. & Oriols, X. (2009). Many-particle hamiltonian for open systems with full coulomb interaction: Application to classical and quantum time-dependent simulations of nanoscale electron devices, *Physical Review B* 79(7): 075315.

Alexander, C., Brown, A., Watling, J. & Asenov, A. (2005). Impact of single charge trapping in nano-mosfets-electrostatics versus transport effects, *Nanotechnology, IEEE Transactions on* 4(3): 339.

Alexander, C., Roy, G. & Asenov, A. (2008). Random-dopant-induced drain current variation in nano-MOSFETs: A three-dimensional self-consistent monte carlo simulation study using "ab initio" ionized impurity scattering, *IEEE Transactions on Electron Devices* 55(11): 3251.

Asenov, A. (1999). Random dopant induced threshold voltage lowering and fluctuations in sub 50 nm MOSFETs: a statistical 3d 'atomistic' simulation study, *Nanotechnology* 10(2): 153.

Asenov, A., Brown, A. R., Davies, J. H., Kaya, S. & Slavcheva, G. (2003). Simulation of intrinsic parameter fluctuations in decananometer and nanometer-scale MOSFETs, *IEEE Transactions on Electron Devices* 50(9): 1837.

Asenov, A., Brown, A., Roy, G., Cheng, B., Alexander, C., Riddet, C., Kovac, U., Martinez, A., Seoane, N. & Roy, S. (2009). Simulation of statistical variability in nano-cmos transistors using drift-diffusion, monte carlo and non-equilibrium greenŠs function techniques, *Journal of Computational Electronics* 8: 349.

Babiker, S., Asenov, A., Cameron, N. & Beaumont, S. P. (1996). Simple approach to include external resistances in the monte carlo simulation of mesfets and hemts, *Transactions on Electron Devices, IEEE* 43: 2032.

Balestra, F., Cristoloveanu, S., Benachir, M., Brini, J. & Elewa, T. (1987). Double-gate silicon-on-insulator transistor with volume inversion: A new device with greatly enhanced performance, *IEEE Electron Device Letters* 8: 410.

Barraud, S., Dollfus, P., Galdin, S. & Hesto, P. (2002). Short-range and long-range coulomb interactions for 3d monte carlo device simulation with discrete impurity distribution, *Solid-State Electronics* 46: 1061.

Blanter, Y. M. & Büttiker, M. (2000). Shot noise in mesoscopic conductors, *Physics Reports* 336(1-2): 1.

Boltzmann, L. W. (1872). Weitere studien uber das wärmegewicht unter gasmolekülen, *Ber. Wien. Akad.* 66: 275.

Brandbyge, M., Mozos, J., Ordejón, P., Taylor, J. & Stokbro, K. (2002). Density-functional method for nonequilibrium electron transport, *Physical Review B* 65(16): 165401.

Bulashenko, O. M., Mateos, J., Pardo, D., González, T., Reggiani, L. & Rubí, J. M. (1998). Electron-number statistics and shot-noise suppression by coulomb correlation in nondegenerate ballistic transport, *Physical Review B* 57(3): 1366.

Collinge, J. P. e. a. (2010). Nanowire transistors without junctions, *Nature Nanotechnology* 5: 225.

Conwell, E. M. (1967). *High field transport in semiconductors, Solid-state Phys. Suppl. 9*, New York Academic.

Datta, S. (1995). *Electronic transport in mesoscopic systems*, Cambridge University Press.

Datta, S. (2005). *Quantum Transport: Atom to Transistor*, Cambridge University Press.

De Mari, A. (1968). An accurate numerical steady-state one-dimensional solution of the p-n junction, *Solid-State Electronics* 11: 33.

Di Ventra, M. (2008). *Electrical Transport in Nanoscale Systems*, first edn, Cambridge University Press, The Edinburgh Building, Cambridge CB2 8RU, UK.

Fischetti, M. V. & Laux, S. E. (2001). Long-range coulomb interactions in small si devices. part i: Performance and reliability, *Journal of Applied Physics* 89: 1205.

Gomila, G., Cantalapiedra, I. R., González, T. & Reggiani, L. (2002). Semiclassical theory of shot noise in ballistic $n^+ - i - n^+$ semiconductor structures: Relevance of pauli and long-range coulomb correlations, *Physical Review B* 66(7): 075302.

Gonzalez, T., Bulashenko, O. M., Mateos, J., Pardo, D. & Reggiani, L. (1997). Effect of long-range coulomb interaction on shot-noise suppression in ballistic transport, *Physical Review B* 56: 6424.

Gonzalez, T. & Pardo, D. (1993). Ensemble monte carlo with poisson solver for the study of current fluctuations in homogeneous gaas structures, *Journal of Applied Physics* 73: 7453.

Gonzalez, T. & Pardo, D. (1996). Physical models of ohmic contact for monte carlo device simulation, *Solid-State Electronics* 39: 555.

Gross, W. J., Vasileska, D. & Ferry, D. K. (1999). A novel approach for introducing the electron-electron and electron-impurity interactions in particle-based simulations, *Electron Device Letters, IEEE* 20(9): 463.

Gross, W. J., Vasileska, D. & Ferry, D. K. (2000a). 3d simulations of ultra-small MOSFETs with real-space treatment of the electron-electron and electron-ion interactions, *VLSI Design* 10: 437.

Gross, W. J., Vasileska, D. & Ferry, D. K. (2000b). Ultrasmall MOSFETs: the importance of the full coulomb interaction on device characteristics, *Transactions on Electron Devices, IEEE* 47(10): 1831.

Gross, W. J., Vasileska, D. & Ferry, D. K. (2002). Three-dimensional simulations of ultrasmall metal-oxide-semiconductor field-effect transistors: The role of the discrete impurities on the device terminal characteristics, *Journal of Applied Physics* 91: 3737.

Gummel, H. (1964). A self-consistent iterative scheme for one-dimensional steady state transistor calculations, *Transaction on Electron Devices, IEEE* 11: 455.

Jacoboni, C. & Lugli, P. (1989). *The Monte Carlo Method for Semiconductor Device Simulation*, Springer-Verlag Wien.

Jacoboni, C. & Reggiani, L. (1983). The monte carlo method for the solution of charge transport in semiconductors with applications to covalent materials, *Review of Modern Physics* 55(3): 645.

Javid, M. & Brown, P. M. (1963). *Field Analysis and Electromagnetics*, McGraw-Hill.

Kurosawa, T. (1966). Proceeding of the international conference on the physics of semiconductors, *Journal of the Physical Society of Japan Supplement* 21: 424.

Landauer, R. (1992). Conductance from transmission: common sense points, *Physica Scripta* T42: 110.

Lundstrom, M. & Guo, J. (2006). *Nanoscale Transistors: Device Physics, Modeling and Simulation*, Springer Science.

Millar, C., Reid, D., Roy, G., Roy, S. & Asenov, A. (2008). Accurate statistical description of random dopant-induced threshold voltage variability, *Electron Device Letters, IEEE* 29: 946.

Oriols, X. (2007). Quantum-trajectory approach to time-dependent transport in mesoscopic systems with electron-electron interactions, *Physical Review Letters* 98(6): 066803.

Oriols, X., Fernández-Diaz, E., Álvarez, A. & Alarcón, A. (2007). An electron injection model for time-dependent simulators of nanoscale devices with electron confinement: Application to the comparison of the intrinsic noise of 3d-, 2d- and 1d-ballistic transistors, *Solid-State Electronics* 51: 306.

Oriols, X. & Mompart, J. (Unpublished). *Applied Bohmian Mechanics: From Nanoscale Systems to Cosmology*, Pan Stanford.

Ramey, S. M. & Ferry, D. K. (2003). A new model for including discrete dopant ions into monte carlo simulations, *Transactrions on Nanotechnology, IEEE* 2: 193.

Reid, D., Millar, C., Roy, G., Roy, S. & Asenov, A. (2009). Analysis of threshold voltage distribution due to random dopants: A 100.000 sample 3d simulation study, *Transactions on Electron Devices, IEEE* 56: 2255.

Reitz, J. R., Milford, F. J. & Christy, R. W. (1992). *Foundations of electromagnetic theory*, Addison-Wesley.

Reklaitis, A. & Reggiani, L. (1999). Monte carlo study of shot-noise suppression in semiconductor heterostructure diodes, *Physical Review B* 60(16): 11683.

Riddet, C., Brown, A. R., Roy, S. & Asenov, A. (2008). Boundary conditions for density gradient corrections in 3d monte carlo simulations, *Journal of Computational Electronics* 7: 231.

Scharfetter, D. & Gummel, H. (1969). Large-signal analysis of a silicon read diode oscillator, *Transaction on Electron Devices, IEEE* 16: 64.

Sverdlov, V., Ungersboek, E., Kpsina, H. & Selberherr, S. (2008). Current transport models for nanoscale semiconductor devices, *Materials Science and Engineering: Reports* 58: 228.

Taylor, J., Guo, H. & Wang, J. (2001). Ab initio modeling of quantum transport properties of molecular electronic devices, *Physical Review B* 63: 245407.

Thijssen, J. M. (2003). *Computational Physics*, Cambridge University Press.

Vasileska, D. & Ahmed, S. (2005). Narrow-width soi devices: the role of quantum-mechanical size quantization effect and unintentional doping on the device operation, *Electron Devices, IEEE Transactions on* 52(2): 227 – 236.

Wordelman, C. J. & Ravaioli, U. (2000). Integration of a particle-particle-particle-mesh algorithm with the ensemble monte carlo method for the simulation of ultra-small semiconductor devices, *Transaction on Electron Devices, IEEE* 47: 410.

Applications of Monte Carlo Method in Science and Engineering
Edited by Prof. Shaul Mordechai

ISBN 978-953-307-691-1
Hard cover, 950 pages
Publisher InTech
Published online 28, February, 2011
Published in print edition February, 2011

In this book, Applications of Monte Carlo Method in Science and Engineering, we further expose the broad range of applications of Monte Carlo simulation in the fields of Quantum Physics, Statistical Physics, Reliability, Medical Physics, Polycrystalline Materials, Ising Model, Chemistry, Agriculture, Food Processing, X-ray Imaging, Electron Dynamics in Doped Semiconductors, Metallurgy, Remote Sensing and much more diverse topics. The book chapters included in this volume clearly reflect the current scientific importance of Monte Carlo techniques in various fields of research.

InTech Europe
University Campus STeP Ri
Slavka Krautzeka 83/A
51000 Rijeka, Croatia
Phone: +385 (51) 770 447
Fax: +385 (51) 686 166
www.intechopen.com

InTech China
Unit 405, Office Block, Hotel Equatorial Shanghai
No.65, Yan An Road (West), Shanghai, 200040, China
中国上海市延安西路65号上海国际贵都大饭店办公楼405单元
Phone: +86-21-62489820
Fax: +86-21-62489821

IntechOpen